Distribution of interplanetary dust detected by the Juno spacecraft and its contribution to the Zodiacal Light

Jørgensen, J. L.; Benn, M.; Connerney, J. E. P.; Denver, T.; Jorgensen, P. S.; Andersen, A.; Bolton, S. J.

Published in:
Journal of Geophysical Research: Planets

Link to article, DOI:
10.1029/2020JE006509

Publication date:
2021

Document Version
Peer reviewed version

Distribution of interplanetary dust detected by the Juno spacecraft and its contribution to the Zodiacal Light

J. L. Jorgensen[1], M. Benn[1], J. E. P. Connerney[2,3*], T. Denver[1], P. S. Jorgensen[1], A. C. Andersen[4], S. J. Bolton[5]

[1]National Space Institute, Technical University of Denmark, Kongens Lyngby, 2800, Denmark.

[2]Space Research Corporation, Annapolis, MD, 21403, USA.

[3]NASA Goddard Space Flight Center, Greenbelt, MD, 20771, USA.

[4]Niels Bohr Institute, University of Copenhagen, Copenhagen, Denmark.

[5]Southwest Research Institute, San Antonio, Texas, USA.

*Correspondence to: J. E. P. Connerney (Jack.Connerney@nasa.gov)

Key Points:

- The Juno spacecraft, in transit from Earth to Jupiter, recorded the impact of interplanetary dust particles on its solar arrays in large numbers.
- The distribution of dust near the ecliptic reveals the influence of mean motion resonances with Jupiter, providing clues to its origins.
- The modeled dust distribution accounts for the variation in Zodiacal light with ecliptic latitude, scattered by the Zodiacal dust bands.

This article has been accepted for publication and undergone full peer review but has not been through the copyediting, typesetting, pagination and proofreading process, which may lead to differences between this version and the Version of Record. Please cite this article as doi: 10.1029/2020JE006509.

Abstract:

The Solar System is home to a cloud of dust that orbits the Sun and makes its presence known by virtue of scattered light (Zodiacal Light) that can be seen after dusk and before dawn. Within this cloud are bands of dust orbiting near the ecliptic plane, evidenced by an excess of scattered light at discrete ecliptic latitudes. Dedicated dust detectors borne by spacecraft in transit of the solar system have detected few such particles of the appropriate size owing to limited detector aperture and sparsity of the population. Thus, the distribution, origin, and orbital evolution of the dust in these bands remains a mystery. A star camera aboard the Juno spacecraft traveling from Earth to Jupiter recorded interplanetary dust impacts on the spacecraft in numbers sufficient to characterize the spatial distribution of such particles for the first time. The observed distribution is consistent with a primary source of dust particles sharing the Mars orbit plane between Earth and the 4:1 resonance with Jupiter. We propose that the primary distribution is scattered by orbital resonances with Jupiter via the Kozai-Lidov (KL) effect into a secondary population at higher inclination to the ecliptic. The measured dust distribution, occupying a volume uniquely determined by the orbital elements of Mars and KL scattering, accounts for the observed variation of the Zodiacal Light with ecliptic latitude. Our results provide a compelling alternative to the prevailing theory of the origin and evolution of interplanetary dust observed at low ecliptic latitudes.

Plain Language Summary:

The Zodiacal light is sunlight reflected by dust in the inner solar system. Variations in the Zodiacal light with ecliptic latitude reveal discrete bands of dust orbiting near the ecliptic plane. The Juno spacecraft, in transit from earth to Jupiter, recorded a sufficient number of impacts with this dust to characterize their distribution in space for the first time. The radial distribution of the dust suggests a primary source of dust with the orbital elements (inclination and eccentricity) of Mars, scattered into a secondary population at higher inclination to the ecliptic. The resulting population accounts for the observed variation of Zodiacal light with ecliptic latitude.

1 Introduction

The space between the planets is populated by objects of various sizes in orbit about the Sun, ranging from minor planets and asteroids to tiny nanograins, with smaller objects more numerous than larger objects over many decades of object radii. The smallest particles are blown out of the solar system by radiation pressure while larger particles drift inward or outward under the influence of Poynting-Robertson drag (Robertson, 1937; Wyatt and Whipple, 1950) and other non-gravitational effects that influence their motion (Burns et al., 1979; Morfill and Grun, 1979; Horányi, 1996; Lhotka et al., 2016; Mann, 2014). The interplanetary cloud of small particles ("dust") must be continuously replenished to offset these losses. This cloud of dust particles can be observed in reflected sunlight (the Zodiacal light), emission of thermal radiation (Hauser et al., 1984; Reach et al., 1997), and samples collected in the earth's upper atmosphere (Love et al., 1994) or in orbit about earth (Love and Brownlee, 1993), but the distribution and origin of the interplanetary dust remains an unsolved problem. However, the well documented variation of the Zodiacal light with ecliptic latitude (Low et al., 1984) evidences the persistence of discrete bands of dust concentrated near the ecliptic plane, implicating a source or sources orbiting in the same plane[s]. It has been widely assumed that the dust bands originate with a few asteroid families that deliver the dust to the inner solar system with the orbital inclination needed to reproduce features in the Zodiacal light curves (Dermott et al., 1984; Sykes, 1987; Dermott and Nicholson, 1989; Sykes, 1990; Dermott et al., 1990; Grogan et al., 1997; Nesvorný et al., 2002; Nesvorný et al., 2003; Nesvorný et al., 2006; Espy et al., 2009). However, in recent years, dust in the Zodiacal cloud contributed by Jupiter family comets (JFCs), Halley-type comets (HTCs) and Oort-cloud comets (OCCs) has received much attention (Nesvorný et al., 2010; Nesvorný et al., 2011; Pokorný, et al., 2014), particularly with regard to larger dust particles that can be tracked entering Earth's atmosphere as radar meteors.

Spacecraft equipped with specialized instruments designed to detect and characterize interplanetary dust particles (IDPs) have traversed the solar system in search of IDPs, detecting the more numerous small particles (<1 μm) that originate beyond our solar system (Humes, 1980; Grün et al., 1994; Landgraf et al., 2000; Horányi et al., 2008; Krüger et al., 2010). Larger IDPs of the size responsible for the Zodiacal light (~1-100 μm) are infrequently collected by these instruments owing to the limited detection aperture (typically ~0.1 m^2) common to such instruments. Thus, larger IDPs have not been detected in-situ in sufficient numbers to characterize their distribution, and as a result, models of the interplanetary dust cloud fitted to variations of the Zodiacal light are poorly constrained.

The Juno spacecraft was launched in August, 2011, bound for Jupiter orbit insertion on July 4th, 2016, on a trajectory that carried it out to the asteroid belt where a deep space maneuver (DSM) sent it back towards a rendezvous with Earth en route to Jupiter (Bolton et al., 2017; Stephens, 2018). Juno was not instrumented with a dedicated dust detection instrument, but it did carry a complement of four star cameras to provide accurate attitude determination for the magnetic sensors (Connerney et al., 2017). This system is known as the Advanced Stellar Compass (ASC) and it employs four Camera Head Units (CHUs), designated A-D, that are collocated with the magnetic sensors. One of these cameras (D) was configured to search for asteroids, recording observations of luminous objects that could be tracked across multiple images in transit across the star background (Soberman et al., 1974; Andersen et al., 2006). This search for "non-stellar objects" (NSOs) turned up a number of luminous objects that were identified as impact ejecta – spallation products excavated from the body of the Juno spacecraft upon impact with an IDP

traveling at ~5 to ~15 km-s^{-1} relative velocity (Benn et al., 2017). IDPs detected in this manner are thought to range from ~1 to ~100 μm in size, representative of the dust population associated with the Zodiacal light (Leinert et al., 1990). Here we present the number of IDPs detected throughout Juno's traverse of the solar system, describe the distribution and orbital evolution of these IDPs in space, and show that this distribution can explain the observed variation of Zodiacal light with ecliptic latitude.

2 Observations

Juno's ability to detect IDP impacts was entirely unanticipated and serendipitous, but in retrospect the spacecraft and instrument were well designed to work together to do just that. Juno was designed to use solar power at Jupiter's orbital distance of 5.2 astronomical units (AU), requiring ~60 m^2 of solar arrays to provide little more than ~600 W of electrical power to the spacecraft and subsystems. The spacecraft also spins (30 or 60 s period) about the +z axis, nearly aligned with the parabolic communication antenna. The magnetometer investigation's star cameras, mounted at the end of one of Juno's three solar arrays, scan the sky with a 13° by 18° field of view (FOV) in the opposite direction, generally anti-sunward (Connerney et al., 2017). Traveling from Earth to Jupiter, Juno was moving with a velocity of >5 km-s^{-1} relative to objects in near-circular Keplerian orbit it might encounter on its way; such objects would impact the anti-sunward side of the solar arrays. Relatively large spallation products (~.1 to ~1 mm in size) ejected from the IDP impact sites were imaged over multiple frames and precisely tracked utilizing the parallax afforded by spacecraft rotation. The detection method is described in detail in Benn et al. (2017) and additional information is provided in the supplementary materials ("Methods"). The evolution of ejecta counts as an IDP impact event, time-tagged, recorded in instrument memory, and stored on the spacecraft awaiting downlink opportunities, typically available once a week during cruise phase. The spacecraft and star camera, in this configuration, together act as a dust detector with ~60 m^2 of aperture, affording a vast increase in collection efficiency relative to dedicated particle detectors flown in space previously.

We confine our discussion to IDPs of the size required to eject spallation products from the target (anti-sunward side of the solar arrays), loosely characterized as IDPs in the size range of ~1 to ~100 μm judging by the size of the spallation products (Benn et al., 2017). The rapid decrease in IDP density with increasing size (e.g., Grün et al., 1994) suggests that most of the IDPs we detect with this method will fall to the low end of this size range (~few to 10 μm). In what follows, when we refer to IDPs, we mean IDPs of the size range that we are capable of detecting. The much smaller dust particles of interstellar origin that have been recorded in significant numbers by dedicated dust detectors flown previously (Humes, 1980; Grün et al., 1994; Landgraf et al., 2000; Horányi et al., 2008; Krüger et al., 2010) are evidently too small to eject spallation products large enough for the CHU to track. This conclusion is consistent with the existence of multiple extended periods of time within which no IDP impact events were recorded; this detection method is insensitive to the flux of small interstellar grains.

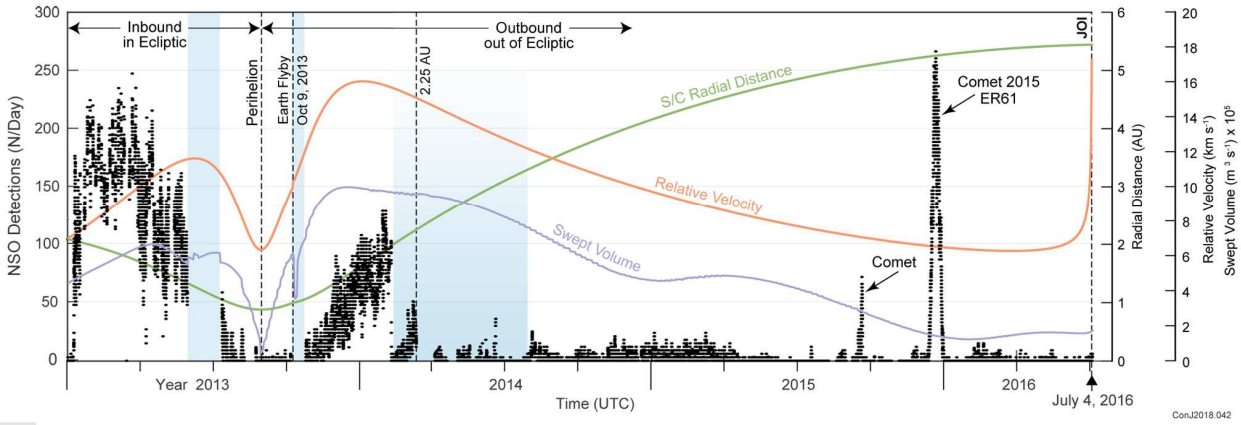

Fig. 1. Overview of IDP impacts as a function of time during the Juno spacecraft's transit from launch to Jupiter orbit insertion. This highly compressed overview shows with black symbols the number of impacts detected per day, with spacecraft direction and significant cruise phase milestones (dashed) noted. Variation of spacecraft radial distance from the Sun (green, right scale), relative velocity with respect to circular orbiting Keplerian objects (tan, rightmost scale), and volume of space swept by the spacecraft (blue, rightmost scale) are illustrated. Extended periods of time lacking observations are identified with solid blue fill; shaded blue fill indicates a period of instrument operation in a different operational mode during which IDP detection was suppressed. The large spikes recorded in 2015 were identified as impact events associated with passage of the spacecraft through the tail of comet 2015ER61, not discussed further in this article.

The number of IDP impact events experienced by Juno along its trajectory from Earth to Jupiter is illustrated in Figure 1. A series of filters was applied to the NSO candidates to isolate IDP impacts, some applied on-board the spacecraft (e.g., object motion relative to the star background) and others in ground data analysis (supplementary material). This process identified a total of 15,278 IDP impacts experienced by Juno during its 5-year cruise to Jupiter. In this process we have undoubtably discarded some actual IDP impact events that left debris trajectories too close to other luminous objects (stars, planets, star clusters) or produced impact ejecta that receded from the spacecraft too quickly.

Interpretation of these data requires a careful consideration of the operation of the instrument and Juno's position relative to the ecliptic plane, and Mars, on its journey to Jupiter (Figure 2). The Juno mission plan included a close Earth flyby (EFB) to impart additional velocity to the spacecraft for its journey to Jupiter. This required a passage from Earth out well beyond the orbit of Mars and into the asteroid belt, where a pair of deep space maneuvers (DSM) were performed prior to Juno's return to Earth for a close flyby (Stevens, 2018). CHU-D was programmed to search for NSOs shortly after the DSMs. Prior to EFB, the search was conducted in the ecliptic plane, as illustrated in Fig. 2. After EFB, Juno's trajectory was inclined to the ecliptic by ~4.5°.

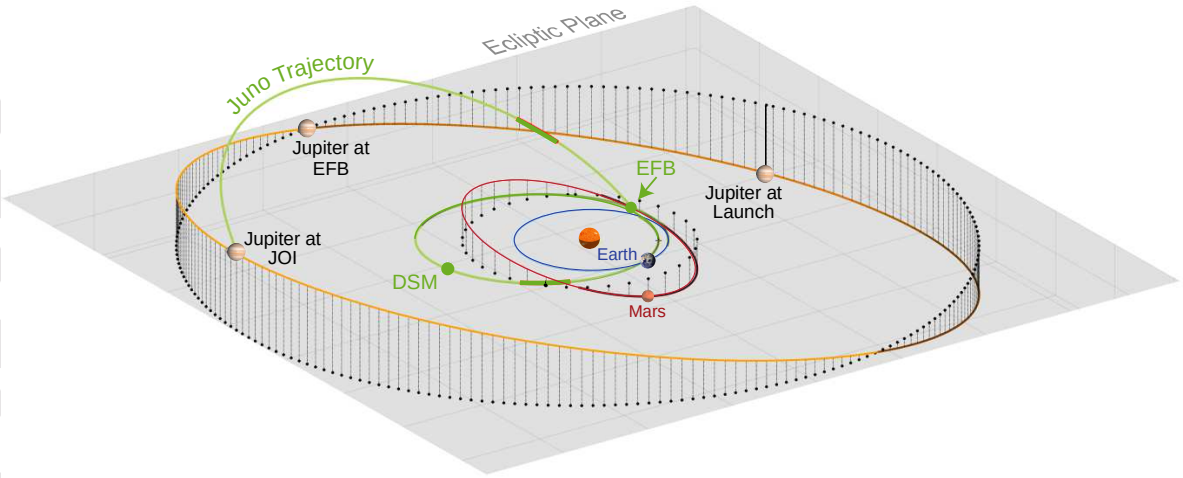

Fig. 2. Illustration of the Juno spacecraft's trajectory from launch (August, 2011) through Jupiter orbit insertion (July, 2016). The orbital position of Jupiter and Mars, and their inclination to the ecliptic, is indicated at 20-day intervals. Juno's trajectory is illustrated (green) with thickened segments illustrating transit of the radial distance range bounded by Mars perihelion (1.36 AU) and aphelion (1.67 AU). Juno remained in the ecliptic while inbound to Earth from DSM and ventured out of the ecliptic while outbound from Earth to Jupiter. Earth and Mars are illustrated as positioned in their orbits at the time of Jupiter orbit insertion (JOI).

It is instructive to examine the IDP detections shown in Fig. 1 as a function of heliospheric radial distance, in the inner solar system, separately, for the inbound (Juno spacecraft traveling towards Earth flyby) and outbound (towards Jupiter) segments of Juno's trajectory. This part of the journey spans radial distances of 0.88 AU (Juno's perihelion) to 2.25 AU. In Figure 3, top, the NSO search begins at the right of the figure, at 2.08 AU, following the final DSM, as Juno exits the main asteroid belt and prior to passage of the radial distance of the 4:1 resonance with Jupiter. Time increases to the left through Juno's perihelion at 0.88 AU. The bottom panel in Figure 3 illustrates the outbound passage from perihelion to the inner asteroid belt, time increasing from left to right.

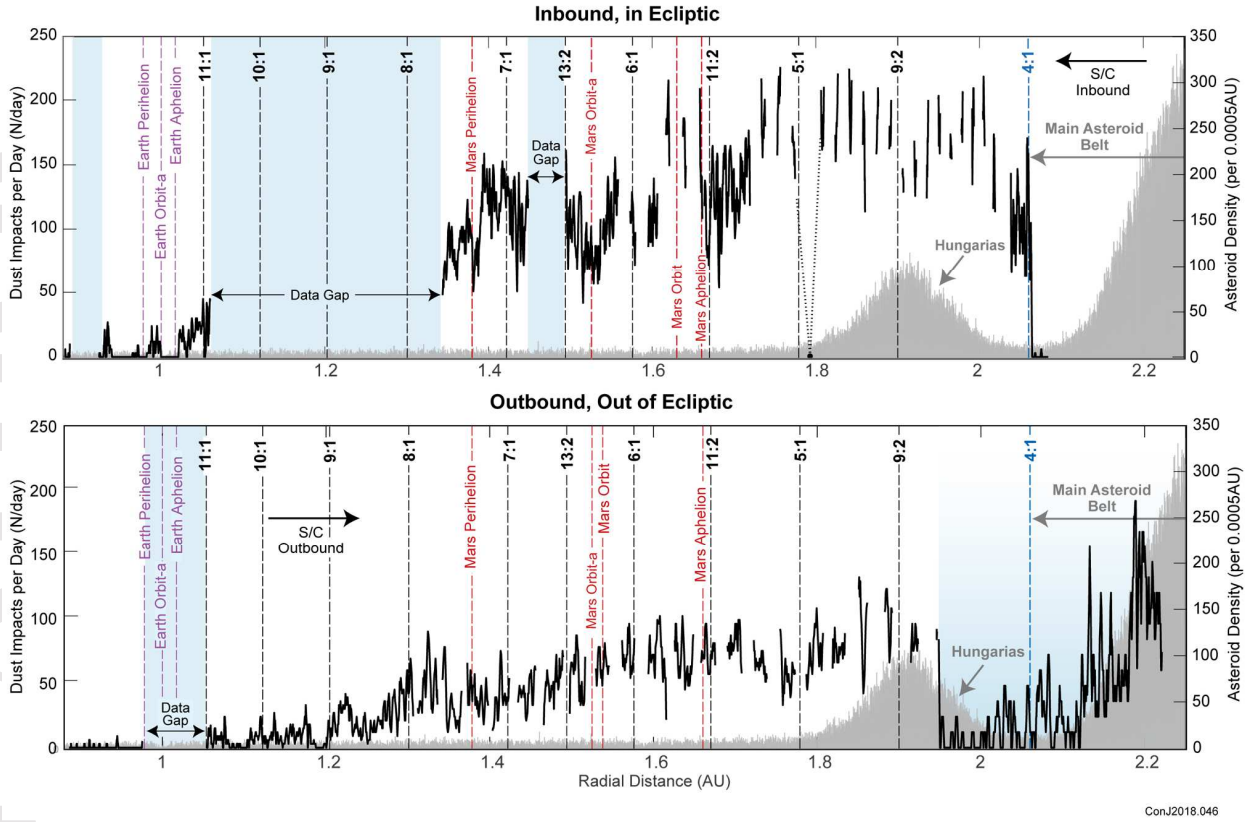

Fig. 3. IDP impacts per day as a function of radial distance from the Sun during the Juno spacecraft's transit, in the ecliptic plane, from the last deep space maneuver (DSM 2) to perihelion (upper) and from perihelion, past Earth flyby, outward (and out of the ecliptic) into the main asteroid belt (lower). Data gap indicated as in Figure 1; blue shaded region identifies instrument operation in a different mode where a correction factor (4x) was applied adjusting the impact rate for the reduced instrument sample rate. For context, asteroid density as a function of radial distance is illustrated with a grey shaded histogram (right scale). The radial positions of mean orbital resonances with Jupiter are identified (ratios, black and blue dashed lines), as are orbit perihelion and aphelion for Earth (purple) and Mars (red).

Both panels in Figure 3 illustrate the variation in IDP impacts as a function of heliocentric radial distance, albeit with numerous small gaps in time. The curves join estimates of the number of impacts per day from eight-hour segments of time-tagged ejecta events. The small gaps between data segments are the result of ASC instrument memory capacity limitations and infrequent data downlink opportunities. When a large number of events are experienced per unit time, the instrument memory fills to capacity and no additional time-tagged events can be logged; the gaps represent the interval of time subsequent to saturation of instrument memory and prior to the availability of memory following NSO data downlink. This instrumental limitation and the regular cadence of downlink opportunities accounts for the regularly spaced data gaps most noticeable along the inbound trajectory between ~1.6 AU and ~2.1 AU, where the largest impact rates were encountered.

3 Analysis

Juno experienced a greater dust impact rate along the inbound transit to EFB, during which the spacecraft remained in the ecliptic plane, relative to the outbound passage traveled at higher ecliptic latitude. Figure 3 presents the data in its most basic form, plotting the number of IDP impacts recorded per day as a function of heliospheric radial distance. To characterize the IDP population density, we require knowledge of the IDP orbits (discussed below) and the projected area of the spacecraft presented to the incoming flux. Allowing for the spacecraft relative velocity and swept volume (supplementary material), the number density of IDPs observed close to the ecliptic plane varies from a few to 8 x 10^{-13} m^{-3}. This agrees well with the density of the 'asteroidal' component of interplanetary dust quoted by Grün et al. (1985; 1997) for IDP masses of 10^{-6} to 10^{-10} g (~few to 50 μm radii). The number density observed at higher ecliptic latitude (4.5°) is about one third of that. Neither panel evidences the 1/r dependence expected of a population of dust drifting inward under the influence of Poynting-Robertson drag (Wyatt and Whipple, 1950; Leinert and Grün, 1990; Mann et al., 2014).

It is also clear that the distribution of events displays more structure during the ecliptic plane transit (upper panel), including an intriguing association with major Jupiter mean motion orbital resonances and the radial range traversed by planets Earth and Mars. In particular, Juno experienced a dearth of impact events (for ~3 weeks) while inbound after DSM, leaving the main asteroid belt, and approaching the strong 4:1 mean motion orbital resonance (MMR) with Jupiter (Figure 3, top panel, read right to left). A large number of events were recorded immediately upon passage inside of the 4:1 resonance, and again after passage inside of the 5:1 resonance (note a single 8-hour period during which no events were recorded just beyond the 5:1 resonance). The dramatic influence of these mean motion resonances on the IDP population suggests that IDPs are efficiently scattered out of orbit at the MMR and that the IDPs we detect reside in low-inclination, near-circular Keplerian orbits. The calculated IDP density (supplementary material) adopts near-circular Keplerian orbits for the IDPs, along with knowledge of spacecraft orientation, to properly account for the relative velocity and directionality of incoming IDPs.

Turning attention to Earth and Mars, as planets that might be expected to sweep dust from their path, we note that IDPs reside comfortably within a putative Mars sweeping region, whereas no IDP impact events were recorded between Earth's aphelion and semi-major axis ("Earth Orbit-a"). We conclude that Earth does effectively sweep its path clear of IDPs with orbits evolving inwards. In contrast, a large impact rate (~200/day) was recorded shortly after passage into Mars' sweeping region and a similarly large rate was experienced just before and after passing through the Mars orbit plane ("Mars Orbit"). Therefore, Mars does not effectively sweep its path clear of IDPs. We do, however, note a systematic decrease in impact events associated with passage through the radial distance equal to Mars's semi-major axis ("Mars Orbit-a"). This may reflect a modest depletion of the IDP population near the mean orbital radius of Mars. No such associations are evident during Juno's outbound passage at higher ecliptic latitude.

The precipitous drop in the IDP population associated with the 4:1 resonance with Jupiter, and at Earth aphelion, suggests that the IDP source resides within this radial range (~1.02 – 2.065 AU) and at low inclination to the ecliptic. It has been widely assumed, if not universally accepted, that the dust interior to the asteroid belt is brought in by asteroid families and/or comets with

eccentric orbits, but if so, such particles would necessarily initially share the orbit eccentricity of the parent body and not survive passage of the orbital resonances with Jupiter as their orbits circularized and slowly evolved inward. The source of the IDP population we measure between Earth and the main asteroid belt must instead reside within the region between Earth aphelion and the 4:1 mean motion resonance with Jupiter (~1.02 – 2.065 AU) where the vast majority of impacts were detected.

Figure 4 shows a substantially reduced impact rate (~10/day) observed in transit through the asteroid belt outwards to Jupiter. This traverse reveals the existence of multiple extended periods of time within which no IDP impact events were recorded. Those associated with the main asteroid belt suggest that asteroids populating the main asteroid belt act largely as a sink, not a source, of IDPs. This is most apparent within the radial range beyond ~2.75 AU to ~3.25 where a few lengthy intervals are found within which no IDP impact events were recorded. The lack of detections during these intervals and on approach to 5 AU also demonstrates that our detection method is insensitive to the omnipresent flux of small *interstellar* grains detected in large numbers by dedicated dust instruments flown throughout the solar system (Mann, 2010). They are evidently too small to eject visible spallation products from the solar arrays. Figure 4 (and to some extent, Figure 3, top panel) also provides some evidence in support of a concentration of dust impact events near orbital resonances, where IDPs may be trapped for an appreciable amount of time (thousands of years) before being ejected (Liou and Zook, 1997). The relatively smaller interplanetary dust population residing in orbits beyond the 4:1 resonance may well be sourced by asteroids and comets in eccentric orbits.

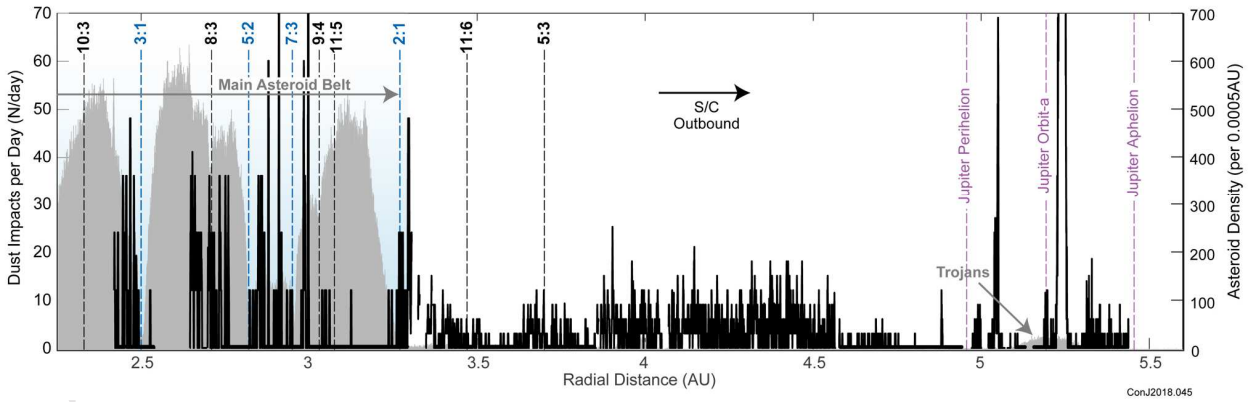

Fig. 4. IDP impacts per day as a function of radial distance from the Sun during the Juno spacecraft's transit, out of the ecliptic plane, from 2.25 AU to Jupiter. Annotations as in Figure 3; note reduced vertical scale for the number of IDP impacts per day.

3.1 Model of Interplanetary Dust Bands

The IDP population observed during the outbound passage after EFB, at an inclination of 4.5° to the ecliptic (Figure 3, bottom panel), is less dense and apparently not significantly influenced by Jupiter resonances or potential absorbers such as Mars. We believe that the population sampled by Juno at higher inclination is a secondary population of IDPs scattered from a primary population with low inclination to the ecliptic by the Kozai-Lidov mechanism (Kozai, 1962; Lidov, 1962). The primary population we associate with Mars, which has an orbital inclination of 1.85°. Over time, dust particles sharing Mars' orbital elements may be expected to fill a

volume of space bounded by +/- 1.85° to the ecliptic and, if drifting inward and outward under the influence of non-gravitational forces (Burns et al., 1979; Horányi, 1996; Lhotka et al., 2016), filling a disc as illustrated in Figure 5.

The Kozai-Lidov effect (KL) is a dynamical gravitational interaction between an orbiting mass (IDP) and a distant third body, in this case, Jupiter. The interaction leads to a periodic exchange of orbital eccentricity and inclination; the maximum inclination (relative to the Mars orbit plane) available to an IDP with Mars' eccentricity is:

$$i = Acos\,[(1-e^2)^{0.5}\cos(i_m)] = 5.5°$$

Where e is Mars' orbital eccentricity (0.0934) and i_m is Mars' inclination relative to Jupiter's orbital plane (1.44°).

The secondary population, if scattered via the Kozai-Lidov effect acting on the primary population of IDPs, will fill a disc-like volume as illustrated in Figure 5 bounded by +/-7.4°, summing Mars' orbital inclination of 1.85° and the KL scattering angle of 5.5°. KL oscillations may be expressed in terms of a pair of binaries, an inner binary consisting of masses m_1 and m_2, and an outer binary consisting of masses m_2 and m_3. In the test particle limit ($m_2 \rightarrow 0$) appropriate to IDPs, to within an order of magnitude, the period for KL oscillation over a complete cycle from maximum eccentricity (and minimum inclination) to maximum inclination (and minimum eccentricity) and back is given by (Antognini, 2015):

$$t_{KL} \cong \frac{8}{15\pi}\left(1+\frac{m_1}{m_3}\right)\left(\frac{{P_{out}}^2}{P_{in}}\right)(1-{e_2}^2)^{\frac{3}{2}} \approx 13{,}000\ years$$

where m_1 is the mass of the Sun (1.99 x 10^{30} kg), m_3 is the mass of Jupiter (1.90 x 10^{27} kg), P_{out} is the orbital period of Jupiter (12 years) and P_{in} is the orbital period of an IDP (1.88 years) leaving the Mars system. IDPs may be expected to achieve maximum inclination to the ecliptic in ¼ of this time, i.e., in about 3,000 years, long before Poynting-Robertson drag can remove an IDP of ~10 μm size (see figure S4).

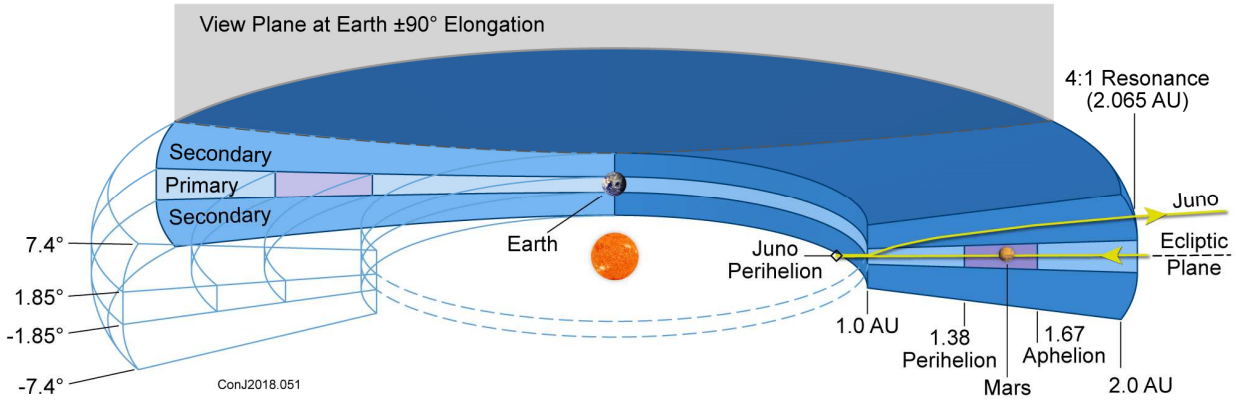

Fig. 5. Illustration of the modeled distribution of IDPs consisting of two distinct populations. A primary (source) distribution exists within 1.85° of the ecliptic plane, originating at Mars, and a

secondary distribution bound by +/- 7.4° is fed by the Kozai-Lidov mechanism operating on the primary IDP population. Juno's trajectory inbound and outbound is indicated (yellow). A radial cut (right) illustrates the two volumes and Juno's trajectory (yellow) through them. A cut in a plane at +/-90° elongation (left) and normal to the ecliptic illustrates the viewing direction of observations from Earth or Earth-orbiting satellites (e.g., COBE, IRAS) observing Zodiacal light.

3.2 Implications for the Zodiacal Light

The IDP distribution we measure, if distributed according to our model, ought to be consistent with the observed variation of Zodiacal light with ecliptic latitude, as measured by instruments on Earth orbiting satellites such as the Cosmic Background Explorer (COBE) and the Infrared Astronomy Satellite (IRAS). Here (Figure 6) we model the intensity of light reflected by the IDP population with that measured (Espy et al., 2009) by IRAS, using a linear approximation to the distribution of IDPs that we measured (supplementary material) and assuming that the density of IDPs that we measure is uniform throughout the primary and secondary population regions illustrated in Figure 5. The IRAS measures the Zodiacal light in a direction orthogonal to a radius vector from the sun as illustrated in Figure 5, left cut, and with that viewing geometry the Zodiacal light intensity is most sensitive to the nearby dust illuminated with more intense sunlight. The two closely spaced peaks near the ecliptic (+/- 1.4°) result from the primary IDP population distributed within +/- 1.85° of the ecliptic. The secondary distribution within +/- 7.4° of the ecliptic populated by Kozai-Lidov scattering of the primary population yields the two peaks (+/- 9.5°) commonly referred to as "the 10° peaks" in the literature.

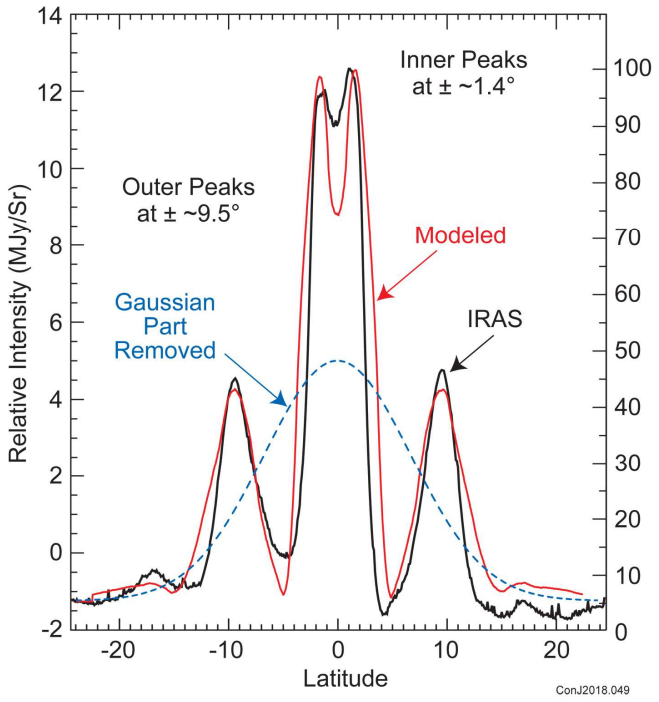

Fig. 6. Contribution of the modeled (red) interplanetary dust bands to the Zodiacal light, compared with the IRAS 25μ intensity variation (Gaussian background removed) with ecliptic latitude (Espy et al., 2009). A Gaussian intensity distribution (blue dashed) was removed from the modeled intensity in approximating the processing applied to the IRAS intensity curve

(supplementary material). The primary source distribution with orbital inclination of +/- 1.85° accounts for the pair of peaks in the Zodiacal light observed at +/- 1.4 degrees about the ecliptic; a secondary distribution with orbital inclination of +/-7.4 degrees (appearing at +/-9.5° degrees as viewed from Earth orbit at +/- 90° elongation) is fed by Kozai-Lidov scattering of the primary distribution.

The approximate total number of IDPs contained in the model distribution illustrated in Figure 5 may be estimated by direct integration (Supplementary materials), yielding $N \sim 2 \times 10^{22}$ particles. Assuming an average IDP mass of ~15 ng, corresponding to a 10 μm radius particle, the detectable IDP population has a mass of $\sim 2.8 \times 10^{11}$ kg. To sustain this population against loss by Poynting-Robertson drag over a time span of ~100,000 years requires a replenishment rate of ~ 30 kg-s^{-1}.

5 Discussion

The population of IDPs we measure presumably reflects a steady state between the supply of IDPs and the loss rate, among other factors that influence detection, such as spacecraft and IDP orbital characteristics, detector (spacecraft) projected area, image sensitivity, and so on. Little is actually known about the supply of IDPs, although it has long been assumed that the IDPs responsible for the Zodiacal light (~1-100 μm) are delivered to the inner solar system by comets and asteroids in elliptical orbit about the sun. The evidence in support of this assumption is largely circumstantial, as this population has until now escaped measurement. Morfill and Grun (1979) summed up the situation well: “an alternative to this is not perceptible to us”.

The loss rate of IDPs depends on many processes affecting their orbital motion as well as those that lead to mass loss, such as sputtering, sublimation, and collisional fragmentation. Orbital motion is influenced by forces that depend critically on particle size, such as (electromagnetic) radiation pressure, Poynting-Robertson drag, solar wind drag, and Lorentz forces on charged dust particles (Burns et al., 1979; Morfill and Grun, 1979; Horányi, 1996; Lhotka et al., 2016). Radiation pressure is effective in quickly clearing some small particles (<~1 μm) out of the solar system, depending on mineralogy and light scattering properties (Burns et al, 1979), but even smaller particles (<~0.1 μm) are cleared primarily by solar wind drag and Lorentz forces (Morfill and Grun, 1979; Horányi, 1996; Lhotka et al., 2016). Radiation pressure and Poynting-Robertson drag are the dominant non-gravitational forces acting upon the Zodiacal IDPs (Burns et al., 1979), yielding to the Yarkovsky effect for larger objects, depending on spin period. Poynting-Robertson drag and the Yarkovsky effect (assuming prograde rotation) both circularize and collapse particle orbits, limiting orbital lifetime (supplementary material). Thus, *in-situ* measurements of smaller (<1 μm) IDPs and inferences drawn from radar studies of larger objects (>400 μm) entering Earth’s atmosphere are of limited use in diagnosing the Zodiacal IDP population; these populations evolve under the influence of very different dynamical effects. The smaller particles measured *in-situ* are mostly of interstellar origin (Landgraf et al., 2000; Mann, 2010).

Our analysis of the IDP population diverges from the usual approach in one key respect: we assume the IDPs we detect are in near-circular Keplerian orbits. This assumption follows naturally from the observation that IDP density at low inclination to the ecliptic drops dramatically just beyond the 5:1 and 4:1 mean motion resonance with Jupiter; IDPs are evidently efficiently ejected from such orbits. This assumption is in contrast to that prevailing since

Dermott et al. (1984) originally attributed the peaks in the Zodiacal light curve to dust bands associated with specific asteroid families (Eos, Themis, and Koronis). These families have orbital inclinations that match what was needed to reproduce the variations observed in the Zodiacal light curve. Thus began modeling efforts of increasing sophistication and complexity, using specific asteroid families (Sykes, 1987; Dermott and Nicholson, 1989; Sykes, 1990; Dermott et al., 1990; Grogan et al., 1997; Nesvorný et al., 2002; Nesvorný et al., 2003; Nesvorný et al., 2006; Espy et al., 2009) and/or Jupiter family comets, Halley-type comets and Oort-cloud comets (Nesvorný et al., 2010; Nesvorný et al., 2011; Pokorný, et al., 2014) to deliver IDPs to the inner solar system. The population we measured demonstrates that IDPs are ejected from orbits just beyond the mean motion resonances with Jupiter; dust delivered by crossing asteroids or comets would not survive inward migration across the resonances. Of course, there are a great many asteroid and comet families, and Reach et al., (1997) questioned why only a few of them produced dust bands. Why not, for example, the Nysa, Flora, and Eunomia/Io asteroid families?

Our IDP model fits these new (and unique) observations and benefits from simplicity. We show that the population we measure along two invariable planes near the ecliptic is consistent with a single source of IDPs with (initially) the orbital elements of Mars, scattered via the Kozai-Lidov mechanism into a secondary volume determined by Mars' orbital elements. Kozai-Lidov scattering occurs well before radial migration of IDP orbits under the influence of non-gravitational forces. We show that this distribution is sufficient to explain the observed variation of the Zodiacal light with ecliptic latitude ("Zodiacal dust bands"). There are no adjustable parameters in this model other than a scaling parameter for the light reflected from individual particles. In contrast, the alternative hypothesis, whereby the Zodiacal dust bands are fed by asteroids and comets transiting the inner solar system, requires identification of one or more asteroid or comet families for each pair of peaks in the Zodiacal light curve. With well over 100 individual asteroid families now identified by examination of their proper elements (Zappalá et al., 1995; Milani et al., 2014), it is perhaps not surprising that some can found with orbital inclinations close to that needed to match the Zodiacal dust bands. However, it is difficult to understand why only some asteroid families – the ones with the required inclinations – contribute dust bands, and not the many others.

What is lacking in our model is a mechanism by which the primary IDP population is created with the inclination and orbital eccentricity of Mars. Can the planet Mars source this population? A large flux of dust particles is observed by the Mars-orbiting MAVEN spacecraft (Andersson et al., 2015) but the source of the dust remains a mystery; the observed distribution is thought to be inconsistent with an origin at either Mars satellite Phobos or Diemos. While Mars does suffer episodic planet-wide dust storms (Martin and Zurek, 1993; Zurek and Martin, 1993) and Mars dust (so-called "rocket dust") is launched to extraordinary altitudes (Spiga et al., 2013; Heavens et al., 2019), escape from Mars would require overcoming escape velocity (~5 km-s^{-1}), for which no mechanism has yet been identified.

Alternatively, the Mars satellites Phobos and Diemos could potentially source dust ejected from the regolith with modest velocity ($v_{esc} \geq 12$ m-s^{-1} for escape from Phobos, less for Diemos). This problem has been considered by many authors following S. Soter's contemplation of a dust ring (torus) formed in orbit about Mars by micrometeoroid bombardment of the Mars satellites (Soter, 1971). Dust of appropriate size (~10 μm to ~100 μm) launched with modest velocity from either satellite can reside in a torus about Mars for thousands of years (Soter, 1971; Krivov, 1994; Krivov and Hamilton, 1997) but escape from the Mars system remains an obstacle and

micrometeoroid bombardment of Phobos and Diemos evidently yields to little ejecta mass by several orders of magnitude (Krivov, 1994). Thus we at present can identify no specific delivery mechanism by which the primary population is seeded.

6 Conclusions

We have measured the density of IDPs as a function of radial distance from the Sun between Earth and Jupiter, and we propose that the circumsolar dust bands of IDPs in our solar system originate in association with the planet Mars, initially sharing the orbital elements of Mars. IDPs are scattered to higher inclinations via the Kozai-Lidov mechanism and subsequently evolve both inward toward the Earth and outward toward the asteroid belt and. We detected a dramatic decrease in IDP density just beyond the 5:1 and 4:1 mean motion resonance with Jupiter and conclude that outward evolving IDPs in near-circular Keplerian orbits are ejected from such orbits. Fewer IDPs are detected within and beyond the main asteroid belt.

The capability to detect dust impacts on the solar arrays continues with Juno in orbit about Jupiter since July 5, 2016. However, few impacts are detected by the ASC during passage through the ring plane; ring particles in prograde orbits would thus far impact the sunward side of the arrays, producing ejecta beyond the CHU field of view. As the orbit evolves in extended mission, dust impacts occurring during a periapsis pass will occur on the darkened side of the arrays, once again visible to the ASC's camera D. It will then be possible to compare the ring particle impact rate with that observed by the Waves investigation (Ye et al., 2020), which is sensitive to smaller particles impacting the spacecraft on any surface. The Waves instrument detects particle impacts by recording the impulsive change in spacecraft potential associated with the high temperature plasma as it evolves from the impact site.

The IDP environment recorded by Juno on its journey to Jupiter has potentially significant implications for the design and qualification of space flight hardware as well as mission design. Solar-powered spacecraft with large projected area have ventured successfully to the outer planets (e.g., Rosetta, Juno) but these spacecrafts used solar arrays backed with relatively massive aluminum honeycomb and carbon composite substrates. The flux of IDP swept by these spacecrafts was absorbed by the anti-sunward side of the solar array substrate. Will the new generation of ultra-thin, flexible solar arrays proposed for upcoming deep space missions tolerate IDP impacts as well?

Acknowledgments: We thank project and support staff at the Jet Propulsion Laboratory (JPL), Lockheed Martin, and the Southwest Research Institute (SWRI), for the design, implementation, and operation of the Juno spacecraft. We also thank staff at Goddard Space Flight Center and the Technical University of Denmark, providing science instruments and support. We especially thank C. Ladd of the Space Research Corporation (SRC) for graphics and presentation support. Contributions of researcher Connerney (NASA/SRC) were supported by contract with the SWRI under contract with NASA (NNM06AA75C). The authors declare no competing interests and no author has an affiliation that may be perceived as a conflict of interest. All data used in this article is available in the main text and in the supplementary materials, as well as in the permanent archival data repository, Zenodo (Jorgensen et al, 2020). JPL manages the Juno mission for the principal investigator, Scott Bolton, of SWRI. The Juno mission is funded by

NASA and is part of the New Frontiers Program managed at NASA's Marshall Space Flight Center in Huntsville, Alabama.

Supplementary Materials:

Materials and Methods

Figures S1-S6

Tables S1

Data S1 filename “IDP_List.txt”

References:

Andersen, A. C., Michelsen, R., Haack, H., et al., (2006). The autonomous asteroid mapping mission "Bering". *Acta Astronautica* 59, 966–973. doi:10.1016/j.actaastro.2005.07.025

Andersson, L., Weber, T. D., Malaspina, D., et. al. (2015). Dust observations at orbital altitudes surrounding Mars. *Science* 350, Issue 6261. doi:10.1126/science.aad0398

Antognini, J. M. O. (2015). Timescales of Kozai-Lidov oscillations at quadrupole and octupole order in the test particle limit. *Mon. Not. R. Astron. Soc.,* 452, Issue 4, 3610–3619. doi:10.1093/mnras/stv1552

Benn, M., Jorgensen, J. L., Denver, T., et. al., (2017). Observations of interplanetary dust by the Juno magnetometer investigation. *Geophys. Res. Lett.* 44, Issue 10, 4701-4708. doi:10.1002//2017GL073186

Bolton, S. J., Lunine, J., Stevenson, D. J., et. al., (2017). The Juno Mission. *Space Science Reviews* 213, Issue 1-4, 5-37, doi:10.1007/s11214-017-0429-6

Burns, J. A., Lamy, P. L., Soter, S. (1979). Radiation forces on small particles in the solar system. *Icarus* 40, 1-48. doi:10.1016/0019-1035(79)90050-2

Connerney, J. E. P., Benn, M., Bjarno, J., et al. (2017). The Juno magnetic field investigation. *Space Sci. Rev.,* 213, Issue 1-4, 39-138, doi: 10.1007/s11214-017-0334-z

Dermott, S. F., Nicholson, P. D., Burns, J. A., & Houck, J. R. (1984). Origin of the solar system dust bands discovered by IRAS. *Nature*, 312, 505-509. doi:10.1038/312505a0

Dermott, S. F., & Nicholson, P. D. (1989). IRAS Dust Bands and the Origin of the Zodiacal Cloud. *Highlights of Astronomy*, (Vol. 8) D. McNally, ed. (Springer, Dordrecht)

Dermott, S. F., Nicholson, P. D., Gomes, R. S., & Malhotra, R. (1990). Modelling the IRAS solar system dust bands. *Advances in Space Research* 10, Issues 3-4, 171-180. doi:10.1016/0273-1177(90)90345-Z

Espy, A. J., Dermott, S. F., Kehoe, T. J., & Jayaraman, S. (2009). Evidence from IRAS for a very young, partially formed dust band. *Planetary and Space Science* 57, Issue 2, 235-242, doi:10.1016/j.pss.2008.06.011

Grogan, K., Dermott, S. F., Jayaraman, S., & Xu, Y. L. (1997). Origin of the ten-degree solar system dust bands. *Planetary Space Sciences* 45, Issue 12, 1657-1665. doi:10.1016/S0032-0633(97)00100-1

Grün, E., Gustafson, B., Mann, I., et al. (1994). Interstellar dust in the heliosphere. *Astron. Astrophys.* 286, 915–924

Grün, E., Zook, H. A., Fechtig, H., & Giese, R. H. (1985). Collisional balance of the meteoritic complex. *Icarus* 62, 244-272. doi:10.1016/0019-1035(85)90121-6

Grün, E., Staubach, P., Baguhl, M., Hamilton, D. P., Zook, H. A., et al., (1997). South-North and radial traverses through the interplanetary dust cloud, *Icarus* 129, 270-288. doi:10.1006/icar.1997.5789

Hauser, M. G., Gillett, F. C., Low, F. J., et al., (1984). IRAS observations of the diffuse infrared background. *Astron. J.* 278, L15-L17. doi:10.1086/184212

Heavens, N. G., Kass, D. M., Shirley, J. H. (2019). Dusty deep convection in the Mars year 34 planet-encircling dust event. *J. Geophys. Res. Planets* 124 doi:10.1029/2019JE006110

Horányi, M., Hoxie, V., James, D., et al. (2008). The student dust counter on the New Horizons mission. *Space Sci. Rev.* 140, 387–402

Horányi, M., (1996). Charged dust dynamics in the solar system. *Annual Review of Astronomy and Astrophysics* 34, 383-418. doi:10.1146/annurev.astro.34.1.383

Humes, D. H. (1980). Results of Pioneer 10 and 11 meteoroid experiments: interplanetary and near-Saturn. *J. Geophys. Res.* 85, 5841–5852. doi:10.1029/JA085iA11p05841

Jorgensen, J. L., Benn, M. B., Connerney, J. E. P., et al. (2020), Distribution of interplanetary dust detected by the Juno spacecraft and its contribution to the Zodiacal Light. (Version 1.0.0) [Data set]. Zenodo. http://doi.org/10.5281/zenodo.3780602

Kozai, Y. (1962). Secular perturbations of asteroids with high inclination and eccentricity. *Astronomical Journal* 67, 591. doi:10.1086/108790

Krivov, A. V. (1994). On the dust belts of Mars. *Astron. Astrophys.* 291, 657-663

Krivov, A. V. & Hamilton, D. P. (1997). Martian dust belts: waiting for discovery. *Icarus* 128, 335-353. doi:10.1006/icar.1997.5753

Krüger, H., Dikarev, V., Anweiler, B., et al. (2010). Three years of Ulysses dust data: 2005 to 2007, *Planetary and Space Science* 58, 951–964, doi:10.1016/j.pss.2009.11.002

Landgraf, M., Baggaley, W. J., Grün, E., et al. (2000). Aspects of the mass distribution of interstellar dust grains in the Solar System from in-situ measurements. *J. Geophys. Res.* 105, 10343–10352. doi:10.1029/1999JA900359

Leinert, C., & Grun, E., (1990) Interplanetary dust, in *Physics of the Inner Heliosphere I*, R. Schwenn, E. Marsch, eds., (Springer-Verlag, Berlin, Heidelberg), pp. 207-275

Levasseur-Regourd, A. C., & Dumont, R. (1980). Absolute photometry of Zodiacal light, *Astron. Astrophys.* 84, 277-279. doi:10.1016/0032-0633(65)90070-X

Lhotka, C., Bourdin, P., Narita, Y. (2016). Charged dust grain dynamics subject to solar wind, Pointing-Robertson drag, and the interplanetary magnetic field. *Astrophysical Journal* 828, No. 10, 10pp. doi:10.3847/0004-637X/828/1/10

Lidov, M. L. (1962). The evolution of orbits of artificial satellites of planets under the action of gravitational perturbations of external bodies. *Planetary and Space Science*, 9, Issue 10, 719-759. doi:10.1016/0032-0633(62)90129-0

Liou, J-C., Zook, H. A. (1997) Evolution of interplanetary dust particles in mean motion resonances with planets. *Icarus* 128, 354-367.

Love, S. G., Joswaik, D. J., & Brownlee, D. E. (1994). Densities of stratospheric micrometeorites. *Icarus* 111, 227-236. doi:10.1006/icar.1994.1142

Love, S. G., & Brownlee, D. E. (1993). A direct measurement of the terrestrial mass accretion rate of cosmic dust. *Science* 262, 550–553. doi:10.1093/mnras/97.6.423

Low, F. J., Beintema, D. A., Gautier, T. N., et. al. (1984). Infrared cirrus: New components of the extended infrared emission. *Astrophysical Journal Part 2*, 278, L19-L22. doi:10.1086/184213

Mann, I. (2010). Interstellar dust in the solar system, Annu. Rev. Astron. Astrophys. 48, 173-203.

Mann, I., Meyer-Vernet, N., Czechowski, A. (2014). Dust in the planetary system: Dust interactions in space plasmas of the solar system. *Physics Reports*, 536, issue 1, 1-39, doi.org/10.1016/j.physrep.2013.11.001

Martin, L. J., & Zurek, R. W. (1993). An analysis of the history of dust storm activity on Mars. *J. Geophys. Res.* 98, 3221–3246. doi:10.1029/92JE02937

Milani, A., Cellino, A., Kneževic, Z., Novakovic, B., Spoto, F., Paolicchi, P. (2014). Asteroid families classification: Exploiting very large datasets. *Icarus* 239, 46-73. doi:j.icarus.2014.05.039

Morfill, G. E., and Grun, E. (1979). The motion of charged dust particles in interplanetary space – 1: The Zodiacal dust cloud, *Planet. Space Sci.* 27, 1269-1282.

Naoz, S. (2016). The eccentric Kozai-Lidov effect and its applications. *Annual Review of Astronomy and Astrophysics*, 1-59, doi: 10.1146/annurev-astro-081915-023315

Nesvorný, D., Bottke, W. F., Levison, H. F., & Dones, L. (2002). A recent asteroid breakup in the main belt. *Nature* 417, 720-722. doi:10.1038/nature00789

Nesvorný, D., Bottke, W. F., Levison, H. F., & Dones, L. (2003). Recent origin of the Solar System dust bands. *Astrophy. J.*, 591, 486-497.

Nesvorný, D., Vokrouhlický, D., Bottke, W. F., & Sykes, M. V. (2006). Physical properties of asteroid dust bands and their sources. *Icarus* 181, 107-144. doi:10.1016/j.icarus.2005.10.022

Nesvorný, D., Jenniskens, P., Levison, H. F., Bottke, W. F., Vokrouhlický, D., & Gounelle, M. (2010). Cometary Origin of the Zodiacal Cloud and Carbonaceous Micrometeorites. Implications for Hot Debris Disks. *Astrophys. J.*, 713, 816-836.

Nesvorný, D., Janches, D., Vokrouhlický, D., Pokorný, P., Bottke, W. F., & Jenniskens, P. (2011). Dynamical Model for the Zodiacal Cloud and Sporadic Meteors. *Astrophy. J.*, 743, 129.

Pokorný, P., Vokrouhlický, D., Nesvorný, D., Campbell-Brown, M., & Brown, P. (2014). Dynamical Model for the Toroidal Sporadic Meteors. *Astrophys. J.*, 789, 25.

Reach, W. T., Franz, B. A., & Weiland, J. L. (1997). The three-dimensional structure of the zodiacal dust bands. *Icarus* 127, Issue 2, 461-484. doi:10.1006/icar.1997.5704

Robertson, H.P. (1937). Dynamical effects of radiation in the solar system. *Mon. Not. R. Astron. Soc.* 97, 423. doi:10.1093/mnras/97.6.423

Soberman, R. K., Neste, S. L., & Lichterfeld, K. (1974). Optical measurements of interplanetary particulates from Pioneer 10. *J. Geophys. Res.* 79, 3685–3694. doi:10.1029/JA079i025p03685

Soter, S. (1971). The dust belts of Mars, *Cornell University Center for Radiophysics and Space Research Report 462*

Spiga, A., Faure, J., Madeleine, J.-B., Määttänen, A., Forget, F. (2013). Rocket dust storms and detached dust layers in the Martian atmosphere. *J. Geophys. Res. Planets* 118, 746–767, doi:10.1002/jgre.20046

Stephens, S. (2018). Juno at Jupiter: The mission and its path to unveiling secrets of the history of the solar system. *IEEE Aerospace Conference*. doi:10.1109/AERO.2018.8396456

Sykes, M. V. (1987). The discovery of more asteroid dust bands: Are they related to asteroid families? *Bulletin of American Astronomical Soc*iety, Vol. 19, p 825

Sykes, M. V. (1990). Zodiacal dust bands: their relation to asteroid families. *Icarus* 85, Issue 2, 267-289. doi:10.1016/0019-1035(90)90117-R

Sykes, M. V., & Greenberg, R. (1986). The formation and origin of the IRAS zodiacal dust bands as a consequence of single collisions between asteroids. *Icarus* 65, Issue 1, 51-69, doi:10.1016/0019-1035(86)90063-1

Wyatt, S. P., Whipple, F. L. (1950). The Poynting-Robertson effect on meteor orbits. *Astrophysical Journal* 111, 134-141

Ye, S.-Y., Averkamp, T. F., Kurth, W.S. et al. (2020). Juno Waves detection of dust impacts near Jupiter, *J. Geophys. Res.: Planets, in press,* doi: 10.1029/2019JE006367

Zappalá, V., Bendjoya, P., Cellino, A., Farinella, P., & Froeschle, C. (1995). Asteroid families: Search of a 12, 487-Asteroid sample using two different clustering techniques. *Icarus* 116, 291-314. doi:10.1006/icar.1995.1127

Zurek, R. W., & Martin, L. J. (1993). Interannual variability of planet-encircling dust storms on Mars. *J. Geophys. Res.* 98, 3247–3259. doi:10.1029/92JE02936